Multishock compression of dense cryogenic hydrogen-helium mixtures up to 60 GPa: Validating the equation of state calculated from first principles

Zhi-Guo Li,[1] Qi-Feng Chen,[1,*] Yun-Jun Gu,[1,†] Jun Zheng,[1] Wei Zhang,[2] Lei Liu,[1,3] Guo-Jun Li,[1,3] Zhao-Qi Wang,[1,3] and Jia-Yu Dai[4,‡]

[1]*National Key Laboratory for Shock Wave and Detonation Physics, Institute of Fluid Physics, P. O. Box 919-102, Mianyang, China*

[2]*School of Science, Southwest University of Science and Technology, Mianyang 621010, China*

[3]*Institute of Atomic and Molecular Physics, Sichuan University, Chengdu 610064, China*

[4]*Department of Physics, National University of Defense Technology, Changsha 410073, China*

(Received 29 March 2018; revised manuscript received 14 June 2018; published 9 August 2018)

Multishock compression experiments on hydrogen-helium (H_2-He) mixtures have been performed via a two-stage light-gas gun for providing equations of state (EOS) covering a wide pressure range. The initial gaseous H_2-He sample was precompressed to 20–30 MPa and cooled down to around 90 K to gain high initial sample density. Up to three shock compressions were clearly observed from the time-resolved light radiance of the shocked sample recorded by a multichannel optical pyrometer. The measured EOS data of the H_2-He mixture reached an unexplored range of pressure up to 60 GPa, which is well in the molecular-to-atomic transition regime. The wide-range experimental data are used to validate the state-of-the-art first-principles simulation methods. It is found that the density functional theory molecular dynamics (DFT-MD) simulations underestimate the dissociation of hydrogen and therefore predict the H_2-He EOS to be stiffer than the experimental data in the molecular-to-atomic transition regime. A careful analysis of the pair correlation functions and comparison with the results of pure hydrogen revealed that DFT-MD might overestimate the effects of helium on the bond of the hydrogen molecule when hydrogen is mixed with helium. Finally, the current measurements validate a linear-mixing *ab initio* EOS [Astrophys. J. Suppl. S. **215**, 21 (2014)] widely used in astrophysics.

DOI: 10.1103/PhysRevB.98.064101

I. INTRODUCTION

Hydrogen and helium are the most abundant elements in the universe. The equations of state (EOS) of hydrogen, helium, and their mixtures under extreme conditions play a fundamental role in modeling astrophysical objects [1–6]. An important category of these objects is the giant planets, such as Jupiter and Saturn of our solar system, which are mainly composed of hydrogen and helium. Modeling the interior structures of giant planets strongly relies on the accurate knowledge about the equations of state of hydrogen-helium (H_2-He) mixtures in a wide pressure-temperature (P - T) range with pressures up to megabar or gigabar ranges and temperatures up to the order of 10^4 K [7,8]. This regime is also well known as the warm dense matter (WDM) regime.

Enormous effort has been made toward building the EOS of H_2-He mixtures for astrophysical implications. An important and widely used EOS for modeling giant planets and brown dwarfs in early times was built by Saumon, Chabrier, and van Horn (SCVH) [9] within the framework of a chemical picture which assumes that bound configurations, such as atoms and molecules, retain a definite identity and interact through pair potentials. Nevertheless, there are some intrinsic approximations that seriously limit the accuracy of the chemical models EOS, such as the treatment of correlations between various species via effective pair potentials and the choice of appropriate reference systems.

In recent years, the quantum molecular dynamics (QMD) or first-principles molecular dynamics (FPMD) simulations, in which electrons are treated quantum mechanically using density functional theory (DFT) and ions are treated as classical particles in Newton equations, have become a much more powerful tool for investigating WDM [10]. Nettelmann *et al.* [11,12] and Militzer *et al.* [13–15] devoted to apply DFT-MD EOS for H_2-He mixtures to giant planets interior models. Militzer *et al.* obtained the H_2-He EOS through the direct DFT-MD simulations of real mixtures. Nettelmann *et al.* performed separate DFT-MD calculations for H_2 and He with subsequent linear mixing treatments for H_2-He mixture EOS, while using chemical models to generate EOS at lower densities and extremely higher temperatures. They both relied on the same exchange-correlation (xc) functional of Perdew, Burke, and Ernzerhof (PBE) [16], however, the obtained EOS were controversial and therefore very different conclusions for Jupiter's interior were derived [17]. It should be noticed that the linear mixing EOS did not take the nonlinear mixing effects into account, which might be the main source of differences between the two EOS [18]. In a much recent work, Becker *et al.* comprehensively compared the linear mixing EOS with the real-mixture EOS and found a remarkably good agreement in the region above 10 kK [19]. Thus, the differences are largely located at pressures below megabar and temperatures below 10 kK. Moreover, this region is well

*chenqf01@gmail.com
†guyunjun01@163.com
‡jydai@nudt.edu.cn

in the molecular-to-atomic (MA) transition regime of the H_2-He mixture, which are generally from ∼1500 to ∼8000 K within the 100 GPa pressure region [18]. Recent experiments suggested that the xc functionals accounting for van der Waals (vdW) interactions would improve the description of the MA transition for pure deuterium [20,21]. For the case of the H_2-He mixture, the presence of helium has a strong influence on the properties of hydrogen [18,22]. The investigations about the effects of vdW interactions for H_2-He EOS in the vicinity of MA transition remain open. Therefore, a detailed discussion about the importance of both vdW and nonlinear mixing effects for H_2-He EOS in the MA transition region is required, besides, accurate experimental EOS data are also necessary for benchmarking these theoretical models.

Shock-compression experiments are paramount in providing the experimental EOS data under high pressure and high temperature conditions and guiding our understanding of computational techniques. However, only few experimental EOS data exist for H_2-He mixtures [23–26], so far up to ∼30 GPa, i.e., far below the pressures at the majority of the interior of giant planets, which significantly limit us to validating the first-principles EOS calculations for H_2-He mixtures. In this work we perform multishock compression experiments on dense cryogenic H_2-He mixtures. The EOS data are measured up to ∼60 GPa, which are directly relevant to the MA transition region of the H_2-He mixture. Motivated by investigating the validation of DFT calculations including vdW functionals and nonlinear mixing effects, we compared these experimental results with DFT-MD simulations using various vdW functionals, as well as the linear mixing EOS. Furthermore, a comparison between our results and that of pure hydrogen is performed, the differences of which reveal the influence of helium on hydrogen molecules in the mixtures.

II. EXPERIMENTS

The schematic diagram of the cryogenic target is shown in Fig. 1. The target mainly consists of a steel sample cell with a front steel baseplate and a rear sapphire window. The steel baseplate is 4 mm thick, which served as the pressure standard for impedance matching measurement. The sapphire

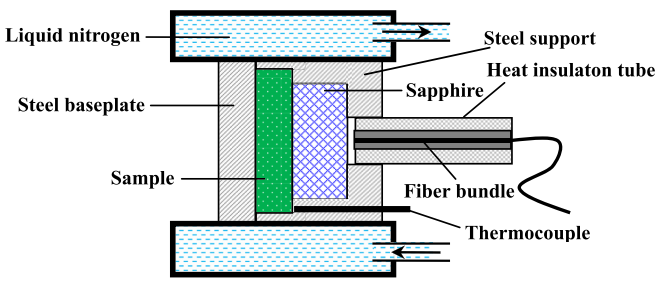

FIG. 1. Schematic diagram of the cryogenic target. The sample is sealed in a cell made up of a steel baseplate, sapphire window, and steel support. A cooling system with a working medium of liquid nitrogen surround the steel sample cell to decrease the initial temperature of the sample, which is measured through a thermocouple thermometer. A fiber bundle, protected by a heat insulation tube from low temperatures, is used to record the self-emission of the shocked sample.

window (single crystal with z-cut orientation), with a thickness of 8 mm, is used to allow the light radiance emitted from the shocked sample to propagate through freely. The steel sample cell, with a thickness of ∼4 mm, was filled with the gaseous H_2-He mixture, which has a mole component of H_2 : He = 1 : 1.2. A circulating cooling system with a working medium of liquid nitrogen surround the steel sample cell to decrease the temperature of the sample through heat transfer. In order to gain high initial densities, before shock compression, the H_2-He gas was precompressed to a dense state with pressures of around 20–30 MPa from an environmental condition by pressurization devices and cooled down to around 90 K, which was measured using a thermocouple thermometer. In our experiments, the initial density ρ_0 of the dense cryogenic H_2-He sample is ∼0.06–0.08 g/cm^3, which is more than double that of previous work by Gu *et al.* [23] and Ternovoi *et al.* [26]. ρ_0 is obtained using a well-established equation of state [27] and the uncertainties in ρ_0 is around 0.2%, which comes from the errors in measuring the pressure and temperature of the dense cryogenic sample. Planar strong shock waves were generated by the impact of high velocity tantalum (Ta) flyers into H_2-He mixture targets, and then were reverberated between the steel baseplate and sapphire window to compress the dense cryogenic H_2-He sample. The Ta flyer, with a thickness of 3 mm, was accelerated to 5.55 km/s via a two-stage light-gas gun with a bore diameter of 30 mm. The velocities of the Ta impactor were measured via a magnetic velocity induction system (MAVIS) with uncertainties within 0.5%. The tilt between the impactor plate and the target face could be controlled within 1°, and the distortion of the impactor during acceleration in the gas-gun launch tube could be neglected. The sizes of the flyer, baseplate, sample cell, and window have been carefully optimized to ensure that the rarefaction and catch-up waves would not compromise the one-dimension character of compression in the optically observed region.

The diagnostics we used is the multichannel optical pyrometer (MCOP) with six wavelength channels [28]. A six-fiber bundle positioned at the central area of the rear sapphire window was used to collect the light radiance emitted from the shocked samples and introduce the light radiance to MCOP. In cryogenic experiments, the effect of low temperature on the fiber and the deposition of ices on the outer window surface are two major factors that will significantly affect the collection of light radiance of the shocked sample. In our experiments, the fiber bundle was surrounded by a heat insulation tube, and was positioned 1 mm away from the window to protect the fiber against the effect from low temperature. Moreover, the issue of the deposition of ices on the outer window surface was solved by vacuumizing the chamber that contains the target. The relatively large sample in these experiments allowed using the fibers with diameter of 62.5 μm. The numerical aperture (N.A.) of the fibers is 0.275. The six channels of MCOP were centered at six wavelengths between 400 and 800 nm. Before each shot, MCOP was carefully calibrated through a standard tungsten light source for shock temperature measurements.

A typical experimental record of the time-resolved light radiance by MCOP for shot 051209 is shown in Fig. 2 (upper panel), which provides a physical picture for the multishock processes. Moreover, a one-dimensional (1D) fluid-dynamics simulation was performed to help understand the MCOP signal

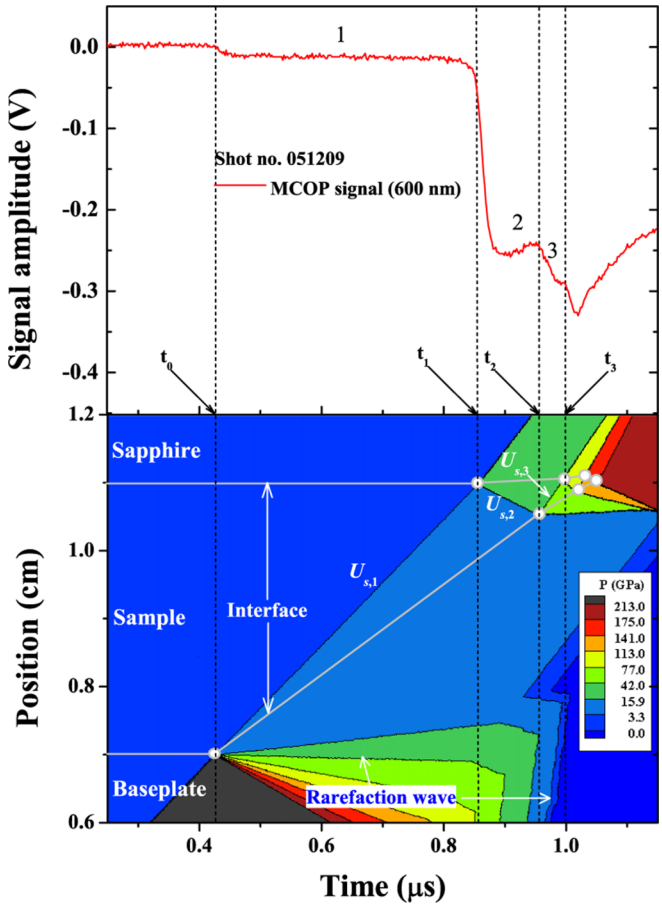

FIG. 2. Upper panel: The measured time-resolved self-emission of the shocked sample by MCOP at a wavelength of 600 nm, which provides clearly the time that the shock wave breaks into sample (t_0) and shock reverberation times at sample/sapphire interface (t_1, t_3) and baseplate/sample interface (t_2). Lower panel: Position-time diagram by 1D hydrodynamic simulations indicating the trajectories of the shock wave front (solid black lines labeled by $U_{s,1}$, $U_{s,2}$, $U_{s,3}$, ...) and interfaces (solid gray lines) of baseplate/sample and sample/sapphire.

and the multishock processes. All initial parameters, i.e., the thicknesses of the flyer, baseplate, sample, and window, used in the simulation were matching the experiments. The position-time diagram indicating trajectories of the shock fronts and interfaces by the simulation is presented in Fig. 2 (lower panel). As can be seen, when the shock produced by the impact between the steel baseplate and Ta flyer reached the baseplate/sample interface (t_0), a rarefaction wave and a shock wave were generated. The rarefaction wave went back into the baseplate and the shock wave entered the sample (the first shock $U_{s,1}$). The first shock drove the sample to a point on the principal Hugoniot and caused a drop of MCOP signal. When the first shock arrived at the sample/sapphire interface (t_1), it was reflected back into the first shocked sample (the second shock $U_{s,2}$), which was reshocked to a state with higher pressure, density, and temperature. The higher sample temperature led to the increase of light radiation intensity, thereby causing a further drop of MCOP signal. Similarly, the second shock was reflected back when it arrived at the baseplate/sample interface (t_2), and compressed the sample for a third time (the third shock $U_{s,3}$). The drop of MCOP signal at t_2 implies that the second shocked sample is still partially transparent so that the light radiance from the third shocked sample can pass through. The above reverberation processes of the shock wave between baseplate/sample and sample/sapphire interfaces would repeat until the sample reached a peak or final state. After time t_3 (the onset of the fourth shock), there were still several reverberation events according to the position-time diagram. However, they were unable to be distinguished from the MCOP signal because the MCOP signal was really complex after t_3, which arose from the sample already became opaque and the light radiance from the shocked sapphire was non-negligible. It should be noted that the MCOP signal did not drop sharply, so there would be a few nanosecond uncertainties when determining the onset of drops in MCOP signals, which resulted in uncertainties for shock transit times. Benefiting from the large sample used in the present experiments, the shock transit times are long. Thus, the uncertainties of shock transit times are relatively small, which are ~1.2%, ~2%, and ~5% for the first, second, and third shocks, respectively. From the position-time diagram, we can also see that the observed multiple reverberation events do not have the influence of the catch-up rarefaction waves.

The multiple shock states can be determined via the impedance matching technique. Figure 3 shows the impedance matching solution for shot 051209. It is convenient to obtain the first shock velocity $U_{s,1}$ according to the first shock transit time $\delta t_1 = t_1 - t_0$ and the thickness of sample cell d_1, where the distortion of cell thickness by the initial high pressure was already included [29]. The particle velocity $U_{p,1}$ can be obtained from the intersection of the first shock compression curve of the H_2-He mixture [$P_1 = P_0 + \rho_0 U_{s,1} U_{p,1}$] and the release isentrope of the steel baseplate which was calculated via the Hugoniot and Grüneisen parameters of the steel baseplate [29]. Then the pressure P_1 and density ρ_1 can be derived by

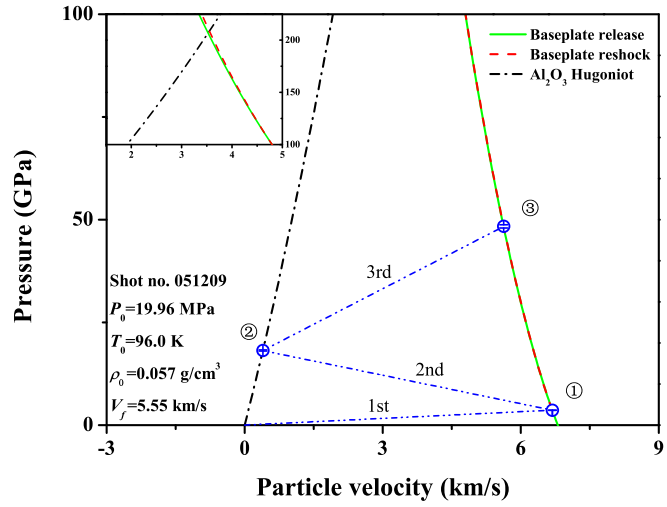

FIG. 3. Impedance matching solution to determine the multiple shock pressures and particle velocities for shot 051209. The open circle symbols indicate the multiple shock states of the current dense cryogenic H_2-He mixture. The blue dash-dot-dot lines represent the first, second, and third shock compression curves of the H_2-He mixture, respectively. The insert shows the situation above 100 GPa.

TABLE I. The initio conditions and the derived multishock states for shots 051209 and 050914. V_f is the velocity of the Ta flyer, P_0, T_0, and ρ_0 are the initial sample pressure, temperature, and density, respectively. P_i and ρ_i ($i = 1, 2, 3$) represent the pressure and density of the sample under the ith shock.

					First shock		Second shock		Third shock	
Shot no.	V_f km/s	P_0 MPa	T_0 K	ρ_0 g/cm^3	P_1 GPa	ρ_1 g/cm^3	P_2 GPa	ρ_2 g/cm^3	P_3 GPa	ρ_3 g/cm^3
051209	5.55	19.96	96	0.057	3.61 ± 0.05	0.202 ± 0.007	18.37 ± 0.32	0.441 ± 0.038	48.51 ± 1.42	0.742 ± 0.120
050914	5.56	27.22	88	0.076	4.84 ± 0.06	0.247 ± 0.008	22.78 ± 0.38	0.521 ± 0.039	57.41 ± 1.55	0.839 ± 0.112

using the Rankine-Hugoniot equations. Similarly, the second shock state is determined by the intersection of the second shock compression curve [$P_2 = P_1 + \rho_1(U_{s,2} - U_{p,1})(U_{p,2} - U_{p,1})$] and the principal Hugoniot of the sapphire window, where the second shock velocity $U_{s,2}$ is calculated through the second shock transit time δt_2 and the distance it traveled $d_2 = d_1 - U_{p,1}(\delta t_1 + \delta t_2)$. During the third shock of the sample, the release baseplate was reshocked by a penetrating shock wave. Therefore, the third shock state is determined by the intersection of the third shock compression curve [$P_3 = P_2 + \rho_2(U_{s,3} - U_{p,2})(U_{p,3} - U_{p,2})$] and the reshock curve of the release baseplate. Here $U_{s,3} = [d_2 + U_{p,2}(\delta t_2 + \delta t_3)]/\delta t_3$ and the reshock curve of the release baseplate can be calculated through the Hugoniot relation and the Grüneisen EOS, by using the release isentrope as a reference curve [30]. The Hugoniot and Grüneisen parameters of the Ta impactor, steel baseplate, and sapphire window were taken from the work of Duffy and Ahrens [31]. The slight increases of initial densities of the steel baseplate and sapphire window due to low temperatures were also considered, which were estimated by their thermal expansion coefficients.

III. RESULTS AND DISCUSSIONS

The initial conditions and the derived multishock states for two shot experiments, 051209 and 050914, are presented in Table I. The experimental pressure and density of the H_2-He mixture are over the range of 4–60 GPa and 0.2–0.8 g/cm^3 from the first to third shock. The resources of uncertainties in shock pressures and densities arise from the uncertainties of the parameters used for the impedance matching calculations. Here the uncertainties of all these parameters, including the initial sample densities, initial sample thickness, velocities of the Ta impactor, shock transit times, and the used Hugoniot parameters for the Ta impactor, steel baseplate, and sapphire window, have been taken into account. We determined the experimental uncertainties through a Monte Carlo technique [32], which is an effective approach for dealing with the propagations of both random and systematic errors in multishock processes. These experimental data are used to validate various DFT-MD EOS with different exchange-correlation functionals, including PBE [16], vdW-DF1 [33], rVV10 [34], and DFT-D2 [35]. The present DFT-MD simulations were performed by using the quickstep code of the CP2K program package, which adopts the hybrid Gaussian and plane-wave (GPW) method to implement fast and accurate DFT calculations [36]. The norm-conserving pseudopotentials of Goedecker, Teter, and Hutter (GTH) [37] are used to describe the electron-ion interaction. The plane-waves cutoff energy is set to 500 Ry, whereas the cutoff energy of the Gaussian type basis set (double zeta valence with polarization, DZVP) is 40 Ry. The Brillouin-zone sampling we used is Γ point only. The cubic simulation box includes 128 atoms (80 H atoms and 48 He atoms) with the periodic boundary condition. It is estimated that the simulations using 128 atoms and Γ point will exhibit finite size errors within 2% and 0.1% for the pressure and internal energy, respectively, through comparisons with larger k points ($2 \times 2 \times 2$) and supercell (containing 256 atoms) calculations. Molecular dynamics were performed in the canonical ensemble with the Nosé-Hoover thermostats [38], and performed for 10 000 steps with a time step of 0.2 fs after 2000 steps thermalization, which is sufficiently long for EOS calculations. The simulation densities range from 0.2 to 1.0 g/cm^3 with a density interval of 0.1 g/cm^3, and temperatures are between 1000 and 10 000 K with a temperature interval of 1000 K.

Figure 4 shows the experimental P-ρ data for shots 051209 and 050914, respectively. Also shown are the results from DFT-MD EOS described above, chemical models of SCVH [9] and the self-consistent fluid variational theory (SFVT) [39,40], a linear mixing *ab initio* EOS by Becker *et al.* (REOS.3) [19], as well as the previous gas-gun data by Gu *et al.* [23]. Gu *et al.* used the gaseous H_2-He mixture as a sample, so the initial sample density (~0.0242 g/cm^3) is much lower than that of present experiments. Therefore, through using the same gas-gun loading technique, the present experiments extensively expand the ranges of EOS for H_2-He mixtures compared with previous gas-gun data, which is more helpful for validating theoretical models, and understanding the intrinsic physics in the molecular-to-atomic phases.

The inset of Fig. 4 are magnified views of the first shock. Only SFVT, SCVH, and REOS.3 results are presented here, because we did not perform DFT-MD simulations below 0.2 g/cm^3, in which the simulation times increase dramatically. It should be mentioned that REOS.3 is an improved version of EOS by Nettelmann *et al.* [11,12], and therefore the EOS data at low densities were generated by chemical models. Within the first shock, the bound species retain their identity and the pair potentials still work, so the chemical models emerge as a useful alternative. It can be seen that the first shock curves by SFVT and REOS.3 calculations are in good agreement with the experimental data. Nevertheless, the result of the SCVH model exhibits small discrepancies. This is likely owing to the used parameters for the pair potentials, which have a substantial influence on the calculation results of chemical models.

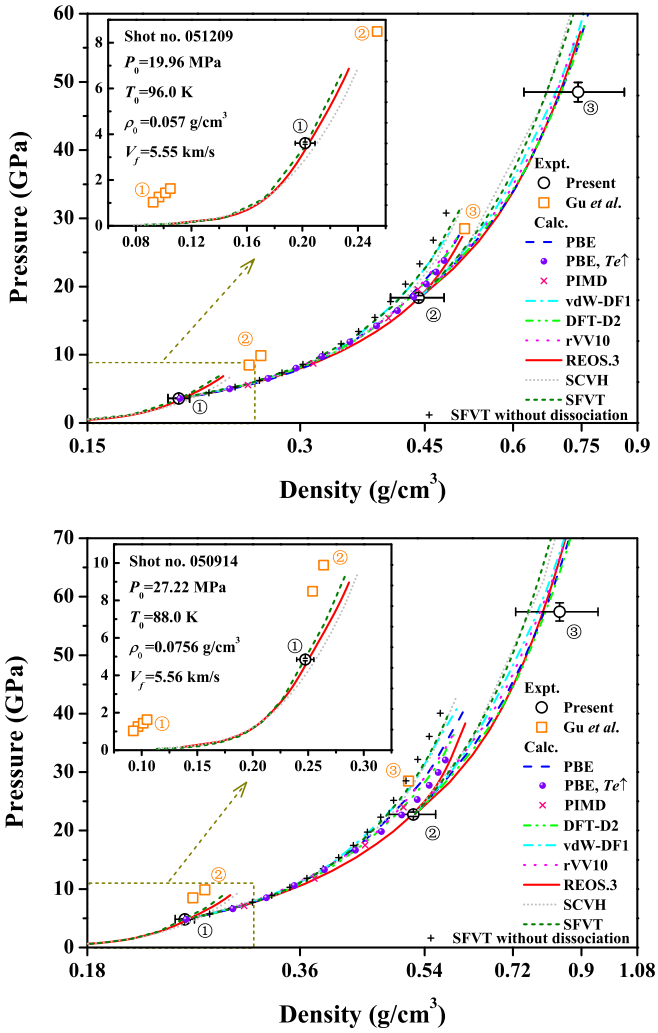

FIG. 4. The first to third shock experimental P-ρ data for shots 051209 and 050914. Open circles represent our experimental data for the dense cryogenic H_2-He mixture. Dashed, dash-dot, dash-dot-dot, and dotted lines are DFT-MD results using PBE, vdW-DF1, DFT-D2, and rVV10 functionals, respectively. The solid circle represents the result by PBE with elevated electronic temperature T_e. The PIMD results are displayed as a times sign (×) symbol. Chemical models of REOS.3, SCVH, and SFVT are displayed as solid, short-dotted, and short-dashed lines, respectively. The SFVT model without the consideration of dissociation is shown by a plus sign (+) symbol. Also shown are the experimental data by Gu *et al.* [23] for gaseous H_2-He mixture with a mole component of H_2 : He = 1 : 1.2 (open squares), and the orange-colored numbers in circles correspond to the shock index in their experiments.

Special emphasis is put on the second shock, within which the MA transition has a strong influence on the EOS. Through the MA transition, the effects of hydrogen dissociation will cause an increase in shock compressibility (ρ_2/ρ_1), resulting in a softer behavior of the second shock curve as energy goes to break chemical bonds. For the purpose of illustration, in Fig. 4, we also present the second shock curve without the consideration of dissociation by using the SFVT model. It can be seen that the SFVT model without dissociation is obviously stiffer than the experimental data. Compared with other theoretical results including dissociation, the SFVT model without dissociation shows agreement at shock pressures below ∼10 GPa, whereas discrepancies appear and increase with rising shock pressures. The onset of the discrepancies is corresponding with the onset of dissociation. In comparison with the experimental data, the second shock curves calculated by the two chemical models of SFVT and SCVH show obvious discrepancies, which may be due to the approximation that various species interacting via effective pair potentials lose effectiveness when the density becomes higher.

The REOS.3, derived with a linear mixing rule by using *ab initio* EOS data, shows reasonable agreement with the experimental data. The separate EOS data of H_2 and He in REOS.3 was generated by DFT-MD simulations with a PBE functional within the second shock. Through a direct comparison between the present PBE result for real mixture and REOS.3, we can evaluate the effects of nonlinear mixing. As can be seen in Fig. 4, REOS.3 is softer than the PBE result. This is due to the fact that the linear mixing neglects the interactions between H_2 and He in the mixture, which makes it easier to be compressed. It is noted that the PBE result is a little stiffer than the experimental data, which is also recognized by the newest quantum Monte Carlo calculations for H_2-He mixtures [41]. Recent experiments on pure deuterium suggested an improved description of the MA transition by exchange-correlation functionals with inclusion of vdW interactions [20,21]. Here we validate three vdW methods of vdW-DF1, DFT-D2, and rVV10 for H_2-He mixtures. It can be seen from Fig. 4 that the second shock curves calculated by three vdW methods are still stiffer than the experimental data. In comparison with PBE, the results with DFT-D2 and rVV10 are close, whereas the vdW-DF1 result is even stiffer.

As discussed above, the increase of shock compressibility through the MA transition is directly related to the hydrogen dissociation. This implies that the stiffer behaviors of PBE (with respect to experimental data) and vdW-DF1 (with respect to PBE) are likely due to the underestimation of dissociation. For DFT-MD simulations, the dissociation of hydrogen molecules can be illustrated by examining the hydrogen pair correlation function (PCF). Figure 5 shows the calculated PCFs of H-H in the H_2-He mixture at the second shock state using the trajectories of PBE, vdW-DF1, rVV10, and DFT-D2 simulations. We also present the PCF result by path integral molecular dynamics (PIMD) to investigate the importance of nuclear quantum effects (NQE) here. In the PIMD simulation, the N-particle quantum system is isomorphic to a classical system consisting of N ring polymers of length P with harmonic intrapolymeric forces. Eight beads ($P = 8$) were used in the present work, and other parameters used in DFT and MD sections are the same as the PBE simulations. It can be found that the hydrogen molecular peak of vdW-DF1 is higher than that of PBE, and the position of the first maximum is smaller than PBE. This suggests that vdW-DF1 predicts more stable hydrogen molecules with short bond length and less dissociation, therefore resulting in stiffer results. The hydrogen molecular peaks of PBE, DFT-D2, and rVV10 are almost identical, and therefore the second shock curves calculated by DFT-D2 and rVV10 are very close to that of PBE. The molecular peak by PIMD is lower than the other DFT-MD

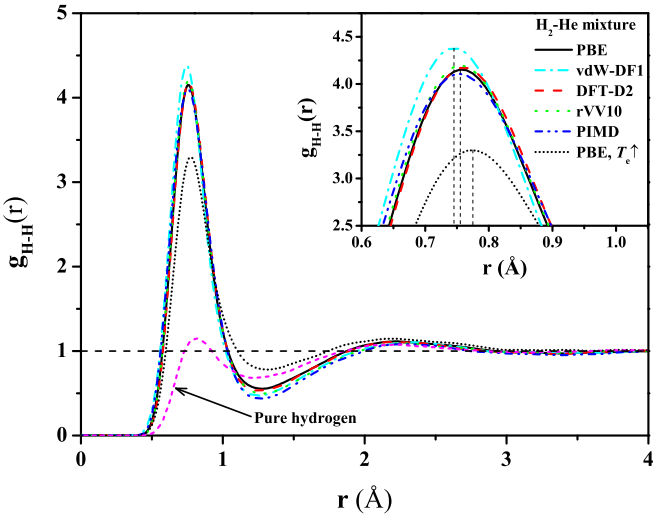

FIG. 5. Pair correlation functions of H-H in the H_2-He mixture at 0.5 g/cm^3 and 6000 K using the trajectories of PBE, vdW-DF1, rVV10, DFT-D2, and PIMD simulations. The black short-dotted line represents the result by PBE with elevated electronic temperature T_e. The magenta short-dashed line is derived from data of pure hydrogen.

results, which implies the inclusion of NQE increases the dissociation. Nevertheless, the increase is very small for the NQE is not really prominent at the present temperature and density conditions. Therefore, PIMD predicts the second shock curves are reasonably consistent with the PBE, rVV10, and DFT-D2 results, as can be seen in Fig. 4. In fact, the NQE will play dominant roles at higher density and lower temperature conditions [42].

In the recent work by Knudson and Desjarlais [20], high precision shock data of pure hydrogen was provided by a magnetically driven shock experiment for evaluating xc functionals. It is worthy to compare our findings with that of Knudson and Desjarlais. Their results show that the vdW-DF1 calculation is stiffer than the experimental Hugoniot of deuterium, which agrees with our conclusions. However, the stiff behavior of PBE with respect to experimental data observed in the present work did not occur for pure deuterium. The PBE calculation is softer than the experimental Hugoniot of deuterium in the MA transition regime, and can well reproduce the peak compression. Such a difference between the H_2-He mixture and pure hydrogen is most probably due to the presence of helium, which has a substantial influence on the stability of hydrogen molecules. And the stiff behavior of PBE for the H_2-He mixture, we suppose, is related to the strengthening of hydrogen molecular bonds in the presence of helium predicted by previous DFT-MD simulations [18,22,43]. To test this hypothesis, we weaken the molecular bonds by increasing the electronic temperature (T_e) as suggested by Knudson and Desjarlais [20]. The elevated electronic temperature T_e we used is two times the ionic temperatures (T_i), i.e., $T_e = 2T_i$. It can be seen from Fig. 5 that the position of the first maximum of PCF by PBE with elevated T_e obviously moves towards the right and the hydrogen molecular peak decreases, which indicates the hydrogen molecular bonds get weaker and the fraction of dissociation increases. Therefore, the second shock curve by PBE with elevated T_e shows better agreement with the experimental data. This also suggests that the effects of helium on the bond of the hydrogen molecule might be overestimated by PBE and vdW funcionals.

For the third shock, a good agreement between PBE and REOS.3 is observed from Fig. 4. This confirms the conclusion by Voberger *et al.* [18] that LM can be considered a good approximation at high temperatures ($T > 8000$ K, close to the third shock temperature). On the other hand, the effects of vdW interactions become negligible at high temperature and high density conditions [44]. In Fig. 4 it can be found that the results of PBE, DFT-D2, and rVV10 functionals converge with increasing shock pressure along the third shock. However, for vdW-DF1, the results are already stiffer compared with others. That is because the vdW-DF1 functional tends to overestimate the bond energy of molecules at high density (but better than the vdW-DF2 functional) [45]. The two chemical models, however, show obvious deviations with the experimental data. The conclusions gained from P-ρ data are also supported by the independent experimental temperature measurements to some extent. A detailed discussion about the inference of shock temperatures from MCOP signals can be found in the Supplemental Material [46].

IV. CONCLUSIONS

We have presented experimental EOS data for a H_2-He mixture covering a wide pressure range of 4–60 GPa through a combined utilization of the multishock compression technique and the dense cryogenic target. The wide-range experimental data are used to validate the current popular theoretical EOS models, including the first-principles methods and the chemical models. Results show that the chemical models emerge as a useful alternative at relatively low densities. In the molecular-to-atomic transition regime, DFT-MD simulations using the PBE functional show better agreement with the experiments than chemical models, but still underestimate the hydrogen dissociation and therefore predict stiffer EOS compared with the experimental data. vdW functionals of DFT-D2, vdW-DF1, and rVV10 which will have influence on the phase transition phenomena [47], however, predict also stiffer EOS results. Analysis of the pair correlation functions revealed that DFT-MD tends to overestimate the effects of helium on the bond of the hydrogen molecule, and we are designing new experiments to gain more accurate EOS data exceeding 100 GPa for further verification of this effect. Finally, the current measurements validate a linear-mixing *ab initio* EOS (REOS.3) widely used in astrophysics, using which we can well reproduce the experimental data. We hope that these insights will provide a guide for future theoretical developments.

ACKNOWLEDGMENTS

This work was supported by the National Natural Science Foundation of China (Grants No. 11674292 and No. 11774429), the National Postdoctoral Program for Innovative Talents (Grant No. BX201700215), the Science Challenge Project (Grant No. TZ2016001), the Science and Technology Development Foundation of China Academy of Engineering Physics (Grants No. 2013A0101001 and No. 2015B0102001),

the President Foundation of China Academy of Engineering Physics (Grant No. 201501032), and the Foundation of Laboratory of Shock Wave and Detonation Physics of China Academy of Engineering Physics (Grant No. LSD-KA1801). D.J.Y. thanks the support of the Advanced Research Foundation of NUDT under Grant No. JQ14-02-01.

[1] N. Nettelmann, R. Redmer, and D. Blaschke, Phys. Part. Nuclei **39**, 1122 (2008).
[2] J. J. Fortney and W. B. Hubbard, Icarus **164**, 228 (2003).
[3] A. Burrows, W. B. Hubbard, J. I. Lunine, and J. Liebert, Rev. Mod. Phys. **73**, 719 (2001).
[4] D. J. Stevenson, Phys. Rev. B **12**, 3999 (1975).
[5] M. A. Morales, S. Hamel, K. Caspersen, and E. Schwegler, Phys. Rev. B **87**, 174105 (2013).
[6] M. A. Morales, E. Schwegler, D. Ceperley, C. Pierleoni, S. Hamel, and K. Caspersen, P. Natl. Acad. Sci. USA **106**, 1324 (2009).
[7] J. J. Fortney and N. Nettelmann, Space Sci. Rev. **152**, 423 (2010).
[8] D. Saumon and T. Guillot, Astrophys. J. **609**, 1170 (2004).
[9] D. Saumon, G. Chabrier, and H. Van Horn, Astrophys. J. Suppl. S. **99**, 713 (1995).
[10] D. Kang and J. Dai, J. Phys.: Condens. Matter **30**, 073002 (2018).
[11] N. Nettelmann, B. Holst, A. Kietzmann, M. French, R. Redmer, and D. Blaschke, Astrophys. J. **683**, 1217 (2008).
[12] N. Nettelmann, A. Becker, B. Holst, and R. Redmer, Astrophys. J. **750**, 52 (2012).
[13] B. Militzer and W. B. Hubbard, Astrophys. J. **774**, 148 (2013).
[14] B. Militzer, Phys. Rev. B **87**, 014202 (2013).
[15] B. Militzer, W. B. Hubbard, J. Vorberger, I. Tamblyn, and S. A. Bonev, Astrophys. J. **688**, L45 (2008).
[16] J. P. Perdew, K. Burke, and M. Ernzerhof, Phys. Rev. Lett. **77**, 3865 (1996).
[17] B. Militzer and W. B. Hubbard, Astrophys. Space Sci. **322**, 129 (2008).
[18] J. Vorberger, I. Tamblyn, B. Militzer, and S. A. Bonev, Phys. Rev. B **75**, 024206 (2007).
[19] A. Becker, W. Lorenzen, J. J. Fortney, N. Nettelmann, M. Schöttler, and R. Redmer, Astrophys. J. Suppl. S. **215**, 21 (2014).
[20] M. D. Knudson and M. P. Desjarlais, Phys. Rev. Lett. **118**, 035501 (2017).
[21] M. D. Knudson, M. P. Desjarlais, A. Becker, R. W. Lemke, K. R. Cochrane, M. E. Savage, D. E. Bliss, T. R. Mattsson, and R. Redmer, Science **348**, 1455 (2015).
[22] J. Vorberger, I. Tamblyn, S. A. Bonev, and B. Militzer, Contrib. Plasma Phys. **47**, 375 (2007).
[23] Y. J. Gu, Q. F. Chen, L. C. Cai, Z. Y. Chen, J. Zheng, and F. Q. Jing, J. Chem. Phys. **130**, 184506 (2009).
[24] P. Loubeyre, R. Le Toullec, and J. P. Pinceaux, Phys. Rev. B **36**, 3723 (1987).
[25] J. A. Schouten, Int. J. Thermophys. **10**, 1 (1989).
[26] V. Y. Ternovoi, S. V. Kvitov, A. A. Pyalling, A. S. Filimonov, and V. E. Fortov, JETP Lett. **79**, 6 (2004).
[27] D.-Y. Peng and D. B. Robinson, Ind. Eng. Chem. Fundam. **15**, 59 (1976).
[28] N. C. Holmes, Rev. Sci. Instrum. **66**, 2615 (1995).
[29] Z.-G. Li, Q.-F. Chen, Y.-J. Gu, J. Zheng, and X.-R. Chen, AIP Adv. **6**, 105309 (2016).
[30] J. Zheng, Q. F. Chen, Y. J. Gu, J. T. Li, Z. G. Li, C. J. Li, and Z. Y. Chen, Phys. Rev. B **95**, 224104 (2017).
[31] T. S. Duffy and T. J. Ahrens, J. Appl. Phys. **82**, 4259 (1997).
[32] M. D. Knudson, M. P. Desjarlais, R. W. Lemke, T. R. Mattsson, M. French, N. Nettelmann, and R. Redmer, Phys. Rev. Lett. **108**, 091102 (2012).
[33] M. Dion, H. Rydberg, E. Schroder, D. C. Langreth, and B. I. Lundqvist, Phys. Rev. Lett. **92**, 246401 (2004).
[34] R. Sabatini, T. Gorni, and S. de Gironcoli, Phys. Rev. B **87**, 041108 (2013).
[35] S. Grimme, J. Chem. Phys. **124**, 034108 (2006).
[36] J. VandeVondele, M. Krack, F. Mohamed, M. Parrinello, T. Chassaing, and J. Hutter, Comput. Phys. Commun. **167**, 103 (2005).
[37] S. Goedecker, M. Teter, and J. Hutter, Phys. Rev. B **54**, 1703 (1996).
[38] S. Nosé, J. Chem. Phys. **81**, 511 (1984).
[39] Q. F. Chen, L. C. Cai, Y. J. Gu, J. Zheng, and G. F. Ji, Phys. Lett. A **374**, 3875 (2010).
[40] Q. F. Chen, Y. Zhang, L. C. Cai, Y. J. Gu, and F. Q. Jing, Phys. Plasmas. **14**, 012703 (2007).
[41] G. Mazzola, R. Helled, and S. Sorella, Phys. Rev. Lett. **120**, 025701 (2018).
[42] D. Kang, H. Sun, J. Dai, W. Chen, Z. Zhao, Y. Hou, J. Zeng, and J. Yuan, Sci. Rep. **4**, 5484 (2014).
[43] Z.-G. Li, W. Zhang, Z.-J. Fu, J.-Y. Dai, Q.-F. Chen, and X.-R. Chen, Phys. Plasmas. **24**, 052903 (2017).
[44] H. Sun, D. Kang, J. Dai, W. Ma, L. Zhou, and J. Zeng, J. Chem. Phys. **144**, 124503 (2016).
[45] R. C. Clay, M. Holzmann, D. M. Ceperley, and M. A. Morales, Phys. Rev. B **93**, 035121 (2016).
[46] See Supplemental Material at http://link.aps.org/supplemental/10.1103/PhysRevB.98.064101 for a detailed discussion about the inference of shock temperatures from MCOP signals, which includes Refs. [9,16,19,29,33–35,39,40].
[47] M. Schöttler and R. Redmer, Phys. Rev. Lett. **120**, 115703 (2018).